JCARME
ISSN: 2228-7922
Journal of Computational and Applied Research in Mechanical Engineering
Vol. 10, No. 1, pp. 125-138
jcarme.sru.ac.ir

Investigation of hot metal gas forming process of square parts

M. Nasrollahzade[a], S. J. Hashemi[b,*], H. Moslemi Naeini[a], Amir H. Roohi[c] and Sh. Imani Shahabad[a]

[a]*Department of Mechanical Engineering, Faculty of Engineering, Tarbiat Modares University, Tehran, Iran*
[b]*Department of Mechanical Engineering, Faculty of Enghelab Eslami, Tehran Branch, Technical and Vocational University (TVU), Tehran, Iran*
[c]*Department of Mechanical Engineering, Faculty of Industrial and Mechanical Engineering, Qazvin Branch, Islamic Azad University, Qazvin, Iran*

Article info:

Type:	Research
Received:	21/07/2018
Revised:	02/04/2019
Accepted:	14/04/2019
Online:	14/04/2019

Keywords:
Gas forming,
High temperature,
Aluminum,
Square cross-section part,
Corner radius.

Abstract

Aluminum alloys are considerably used in automotive and aerospace industries because of their high strength to weight ratio. In this manuscript, the gas forming process of aluminum AA6063 tubes at high temperatures up to 500°C is investigated, through experimental and numerical tests. An experimental setup is prepared, and tube specimens are formed in a die with a square cross-section. Finite element simulation of the hot gas forming process is carried out to investigate the effects of process parameters including the time period of forming process, temperature, and loading path. Uniaxial tensile tests under various temperatures and strain rates are performed in order to obtain flow stress curves of the material. Corner radius and thickness distribution of tubular formed parts is investigated. The results show that smaller corner radii could be formed at higher temperatures, whereas lower forming pressure is necessary. Increasing the time period of the process enhances the corners of the specimens to be formed. In addition, the maximum formability is obtained when the gas pressure increases rapidly at the beginning of the process. However, the increasing rate of gas pressure must be reduced to form a smaller corner radius.

1. Introduction

The crisis of fuel consumption has emerged through the 21st century. As vehicles are major fuel consumers, automotive and aerospace industries seek alternative ways to control the consumption of the fuel. One of the effective ways in this regard is to reduce the weight of vehicles. It also helps to decrease air pollution and greenhouse gases [1]. Nowadays, there is a huge competition to use the materials having high specific strength in the automotive industry and other industries [2]. Aluminum alloys are widely used because of their high specific strength and also their capability for energy absorption. The high percentage of alloying elements in aluminum alloys is the main reason of their low formability. Thus, the application of these materials is limited currently [3]. A proper way to solve this problem is to form these materials at higher temperatures [4].

The Warm Hydroforming (WHF) is a modern forming approach, which is used to form aluminum alloys in automotive industries. In recent years, the warm hydroforming process has

*Corresponding author
Email address: j_hashemi@tvu.ac.ir

been investigated by many researchers. Keigler et al. [5] investigated the formability, thickness distribution, and microstructure of the specimens, before and after the WHF process. Yi et al. [6] used a combined heating system, including an induction coil around the tube and heating element located inside the tube. Hi et al. [7] studied the deformation behavior of magnesium alloy AZ31B tubes in both longitudinal and circumferential directions. Based on their results, the longitudinal formability increases at high temperatures while the circumferential formability decreases at a specific temperature range. Hashemi et al. [8] investigated the thickness distribution of hydroformed aluminum alloy AA1050 tubes at high temperatures and found that the thickness distribution uniformity increases at temperatures above 200°C. Kim et al. [9] simulated the warm free bulge process of aluminum tubes using finite element code Deform-2D. They investigated heat transfer between the die and the tube. Hashemi et al. [10] predicted the forming limit diagram (FLD) of aluminum tubes at high temperatures using modified ductile fracture criteria and Zener-Hollomon parameter in the simulation of WHF process. Abedrabbo et al. [11] developed a temperature-dependent anisotropic material model in the finite element analysis. Using this new model, the forming process of two automotive aluminum alloys (i.e. AA5182-O and AA5754-O) from room temperature up to 260°C was simulated. This developed thermo-mechanical constitutive model predicted accurately both the deformation behavior and failure location in the blank.

Prior investigations show the hydroforming process could be applied only at room temperature up to 300°C. This limitation is due to the lack of appropriate and efficient fluid at higher temperatures [12]. Thus, the hydroforming process is limited to form the complex shape and large deformations. Moreover, cold hydroforming needs a higher pressure of the fluid, and as a consequence, bigger and more expensive tools and fittings. In order to overcome these limitations in the WHF process of aluminum and magnesium tubes at high temperatures (higher than recrystallization temperature), another fluid (air or inert gases such as argon, nitrogen, or carbon dioxide) must be used for applying internal pressure. This process is called hot metal gas forming (HMGF). Naka et al. [13] investigated the effects of forming speed and temperature on the FLD in stretch-forming tests. The results showed that limit strain increases drastically with decreasing speed, while at room temperature, the FLD is not so sensitive to the speed. Also, improvements in the formability at 300°C and low forming speed are specifically due to the high strain-rate hardening characteristics, while below 200°C the formability is strongly affected by strain-hardening. Verma et al. [14] developed an FE methodology based on a two-mechanism material constitutive model to simulate the high-temperature forming of magnesium alloy AZ31 sheet. The FE simulations predicted the thinning of the magnesium alloy sheet with reasonable accuracy. However, the material model fails to accurately track the forming rate near sheet rupture in the free-form bulge forming at the lowest gas pressure. He et al. [1, 4] investigated the formability and microstructure of aluminum alloy AA6061. In addition, the fracture mechanism in the HMGF for bulging aluminum tubes was studied at temperature ranges 350°C-500°C. The results showed that the fracture mechanism at high temperatures was due to the accumulation of micro-pores. Also, three types of longitudinal fracture, peripheral, and random directions occur. Maeno et al. [15-16] investigated the HMGF of aluminum tube to have bulged at elevated temperatures up to 400°C. They also investigated the effects of internal pressure, and the intensity of the electric current on the expansion ratio. Results show that the lower heat conduction of the die improves the corners filling. Lee et al. [17] studied the effect of material microstructure on the mechanical properties and formability of AZ31 alloy, by applying uniaxial tensile test at room temperature and 400°C and biaxial tensile test at 400°C. They observed that the twin density, dislocation density, and grain size are effective on the mechanical properties of the AZ31 alloy at room temperature. While the mechanical properties are only affected by initial grain sizes in the temperatures higher than 400°C. Paul and Strano [18] investigated the effect of process parameters on the hardness and quality of the steel specimens produced by the HMGF process. They observed that hardness is mostly dependent on the pressure-temperature curve in areas that need calibration; moreover, hardness is dependent on tool temperature in the areas which contact quickly with the die. Wu et al. [19-20] formed Ti-3Al-2.5V titanium alloy tubular components with a 70% expansion ratio when the temperature differences are 0, 50, and 15°C using a non-uniform temperature gas forming experimental device. They examined the effect of temperature distribution on the deformation behavior, thickness, microstructure, and mechanical properties of the material. Results show that a suitable temperature difference between forming zone and transition zone is beneficial for axial feeding, which promotes the thickness distribution uniformity. In addition, the best loading path to form a tubular component was achieved at 800°C. Kim et al. [21] used a ductile fracture criterion based on the Zener-Hollomon parameter to predict failure in the hot gas forming process. Fan et al. [22] studied the effect of hot gas forming integrated heat treatment on the microstructure, texture, and hardness of formed parts. They showed that the process must be rapid for higher formability. Wang et al. [23] studied free bulging of titanium alloy TA15 tubes by internal gas pressure at 800°C. They concluded that if the strain rate is constant during the forming process, a maximum of the bulging ratio can be achieved. Wang et al. [24] produced metal bellows by superplastic forming. They used internal gas pressure with axial feed during the forming process. Neugebauer and Schieck [25] developed a hat gas forming setup for forming high strength steel tubes with a maximum gas pressure of 80 MPa and a maximum temperature of 1000°C. Liu et al. [26] investigated corner filling in the hot gas forming process of titanium tubes in a square cross-sectional die. They also studied feeding effect [27] on the hot gas forming of low strength titanium alloy tubes, which demonstrated that the best temperature for higher formability is about 800°C. Maeno et al. [28] used a resistance heating system in the hot gas forming process of aluminum alloy tubes. By this heating method, the temperature remained constant during the forming process. Vadillo et al. [29] used numerical simulation to study the effect of the loading curve in the HMGF process. They could bulge ferritic stainless steel up to 55% at 1000°C. The simulation of the HMGF process was done by Rajaee et al. [30]. They obtained a process window of the HMGF process of AA6063 tubes using Abaqus software. Wu et al. [31] studied the forming behavior of Ti22Al24.5Nb0.5Mo rolled sheets by uniaxial tensile and hot gas bulging tests. They obtained forming limit carve under constant equivalent strain rate. Anaraki et al. [32] investigated the effect of pulsating pressure on formability in hot gas forming. Their results show that pulsating pressure can improve the thickness distribution along the tube.

So far, there are no precise investigations to predict the deformation behavior of the material using the finite element method in the HMGF process. Also, most of the studies are carried out on simple shapes, such as the symmetrical bulge of the sheets and tubes. In this manuscript, the hot gas forming process of aluminum alloy AA6063 tubes is simulated. Numerical results are compared with experimental ones. On the other hand, a hot gas forming system is designed and the experimental deformation of circular tubes into square-shaped is investigated. The effect of process parameters including forming pressure, time period of the forming process, temperature, and initial thickness of the tube on the corner radius, and thickness distribution of the final products are specified.

2. Experiments

The forming of the AA-6xxx alloy is taken into consideration due to good corrosion resistance, high strength to weight ratio, high applications in the automotive industry, and significant formability at high temperatures. Aluminum tubes with an initial external diameter of 40 mm and an initial thickness of 1.5 mm is utilized. All the tubes are seamless. Initial tubes are extruded and their mechanical properties are not changed after the extrusion process; because no heat treatment is applied. The chemical composition of the tubes is determined by quantometer test, which is listed in Table 1. According to the obtained chemical composition, the material of the tube is AA6063 alloy.

2.1. Mechanical properties experiments (tensile test)

Tensile specimens are prepared using a WireCut machine and then, uniaxial tests are performed according to ASTM-E8M using the machine shown in Fig. 1, which made by santam company, in order to obtain the stress-strain diagram of the tube material. Experiments are conducted at 25°C, 400°C, and 500°C. The strain rate ranges are chosen at three different amounts of 0.1, 0.01, and 0.001 s-1 (that is, simulation results show the strain rate in this process is under 0.1s-1 and the stress changes are linear). Fig. 2 shows the obtained true stress-strain curves. The results show that the fracture strain of AA6063 increases 233% and 300% at the temperatures 400°C and 500°C, respectively, in comparison to that of the room temperature. In fact, the flow stress decreases significantly as a result of the softening phenomenon, and the material show no strain-hardening behavior at the temperatures higher than 400°C. Thus, the formability of the tube increases, and lower pressure is necessary to form the material.

Fig. 2 (a) shows an increase in the AA6063 stress in the room temperatures by increasing the strain, due to the strain hardening. On the other hand, after the elastic deformation occurs at the higher temperatures, stress reaches a steady state. This is because of an equilibrium occurs between work-hardening and strain-softening at high temperatures. In fact, the phenomena of dynamic recovery and dynamic recrystallization occur and cause the strain-softening in the material. Flow stress decreases with increasing the strain due to strain-softening behavior (SSB). Fig. 2(a) also shows that the AA60663 tube properties is not dependent on the strain rate. Fig. 2(b) and (c) shows that the strain rate is an important parameter of the material properties at the elevated temperatures, and the stress is defined according to Eq. 1.

$$\bar{\sigma} = K\bar{\varepsilon}^{n} \cdot \dot{\bar{\varepsilon}}^{m} \qquad (1)$$

where, $\bar{\sigma}$, $\bar{\varepsilon}$ and $\bar{\varepsilon}$ are equivalent stress, strain and strain rate, respectively. K, n, and m are strength coefficient, strain-hardening exponent, and strain rate, respectively.

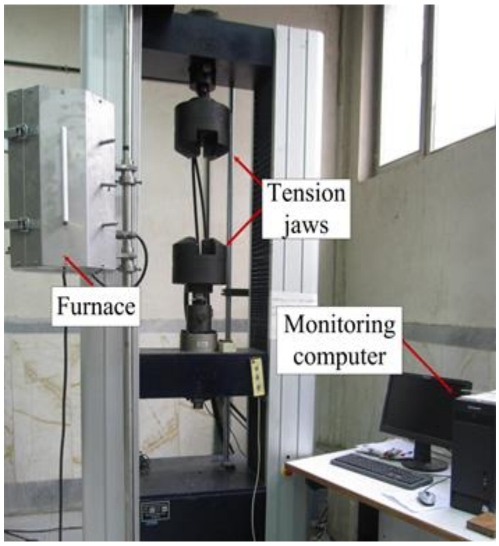

Fig. 1. Tensile test machine.

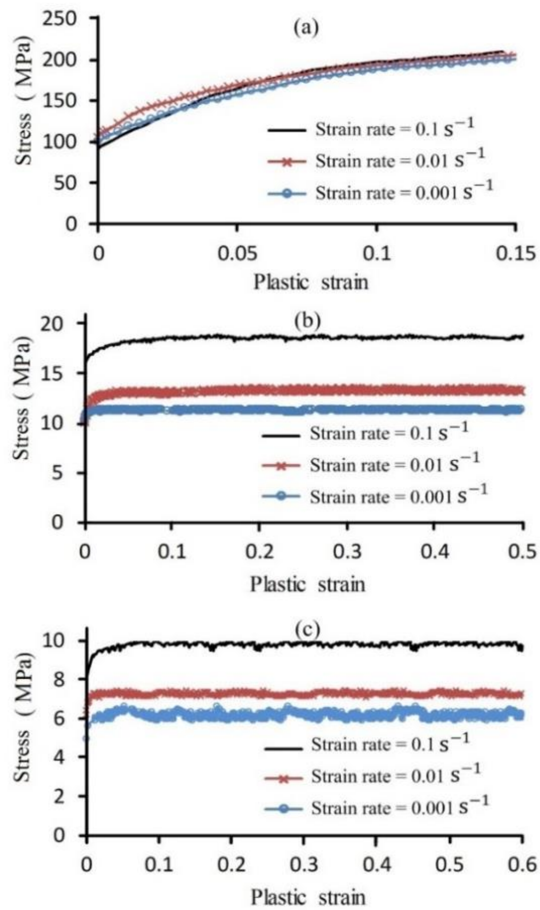

Fig. 2. True stress–strain curves at different temperatures; (a) 25°C; (b) 400°C; (c) 500°C.

Table 1. Chemical composition of the tube.

AL	Mg	Si	Fe	Zn	Cu	Mn	Pb	Ti	Sn	Ni	Ga
Base	0.47	0.44	0.30	0.08	0.06	0.03	0.03	0.03	0.017	0.02	0.01

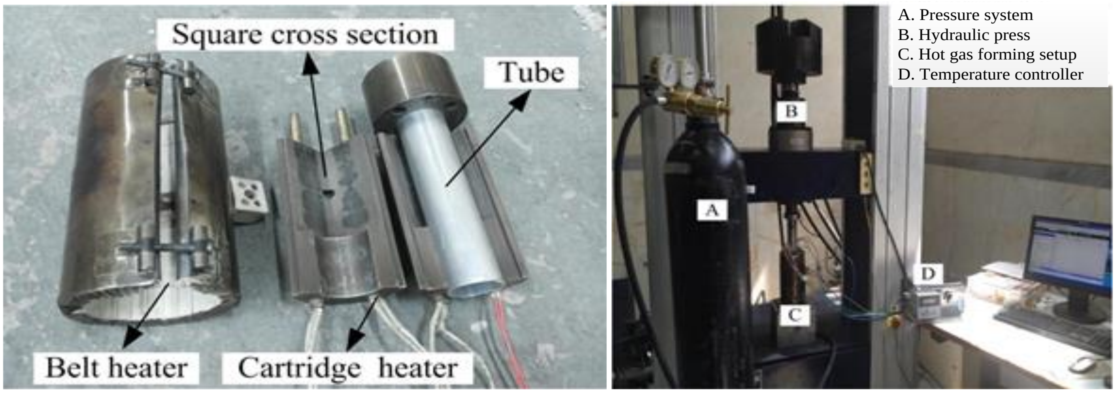

Fig. 3. Components of the hot gas forming setup, hydraulic press and control system.

2.2. Hot gas forming setup

The hot gas forming setup (Fig. 3) for high temperatures is designed in order to produce a square section tubular part with circular ends. Two types of heater are utilized to obtain the desired temperature; (a) belt heater with a power of 1200 W located around the die, and (b) four cartridge elements with a power of 200 W located in the longitudinal direction. Thus, all die parts reache the same temperature, using this combined heating system, and the maximum temperature difference is observed equals to ±5 degrees. The die is made from MO40 alloy steel. The hardness number of die material is 250 based on the Brinell hardness test at room temperature. The die has two circular ends with the diameter of 40 mm. The square part of the die, located between two circular ends, has the square sides equal to 45 mm and the length of 100 mm in the axial direction. At the beginning, the tube is located in the square die shown in Fig. 3. The tube is fixed in its position during the process, and two metallic cones are located at the ends of the tube to achieve an appropriate sealing.

The sealing force on the metallic cones is supplied by a hydraulic press, shown in Fig. 3. Schematic image of the sealing type is shown in Fig. 4. In the next step, the heating system raises the temperature of the die and tube to the desired temperature.

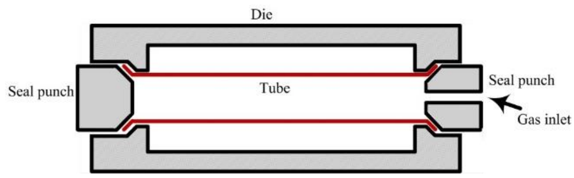

Fig. 4. Sealing type.

The temperature is measured using a K-type thermocouple and is controlled by a temperature control system. After reaching the desired temperature, the internal pressure is applied by a nitrogen cylinder and controlled by a regulator shown in Fig. 3. The rate of pressure increase is linear in all the experiments.

3. Numerical simulation

The process is modeled in ABAQUS 6-13 software using ABAQUS/implicit code. The aluminum tubes used are AA6063 alloy without any heat treatment. Fig. 5 shows the dimensions of the die and the finite element model of the process. The die and tube are symmetrical with respect to three planes; therefore, only 1/8 of the process configuration is modeled. The shell elements are used to discrete the tube, because the thickness to radius ratio of the tube is less than 0.1 [16-18]. Also, the die is modeled as a discrete rigid body. The tube is meshed using S4RT elements (four-node element using the reduced integration method). The effect of element size (3mm, 2mm, 1mm, and 0.7mm) on the simulation results is studied.

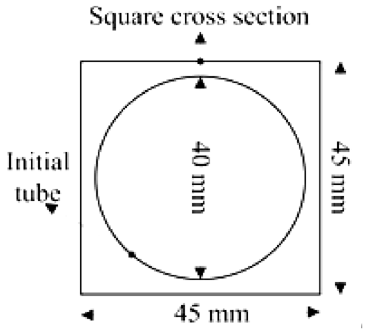

(a)

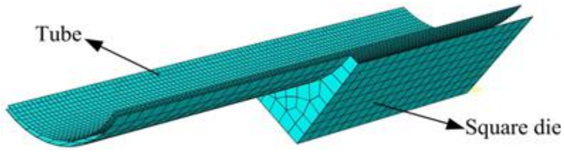

(b)

Fig. 5. (a) Square die dimensions and (b) finite element model of the process.

Thickness distribution in the peripheral direction in the middle cross-section of the parts, at the end of the forming process, is shown in Fig. 6 for the above-mentioned element sizes. The loading condition is also maintained at the same level in four cases. There is a very small variation between the results corresponding to the element sizes of 1mm and 0.7mm. Therefore, the element size of 1mm is utilized in all simulations. The contact between the external surface of the tube and die is defined as a standard surface-to-surface contact, based on the Coulomb friction model. The friction coefficient between the outer surface of the tube and die is measured experimentally. Based on the experiment, friction coefficient is considered 0.15.

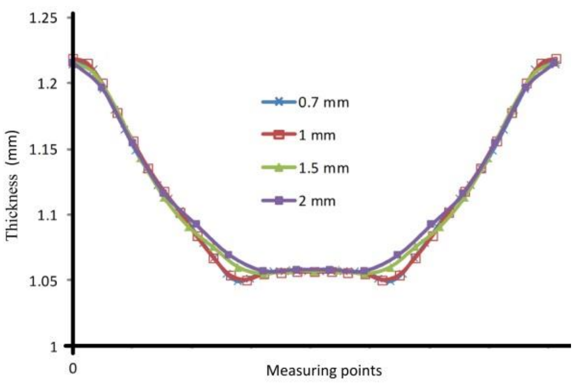

Fig. 6. Effect of element size on thickness distribution.

Material properties are obtained from uniaxial tensile tests and the true plastic stress-strain data are shown in Fig. 2. The isotropic hardening model is implemented for tube deformation in the simulations. Other properties, used in the simulation, are listed in Table 2. The simulation is performed in the form of coupled temperature-displacement analysis, and all parts are assumed to have the same temperature. The gas pressure is defined with a surface uniform pressure, according to the predefined path on the internal surface of the tube.

Fig. 7 (a) shows the thickness distribution of the specimen, obtained from the FE simulation of the process at 500°C, and the maximum internal pressure of 12 bar. It is obvious that the minimum thickness induces in the corner of die, at the beginning part of the transitional circular-to-square zone. The experimental results also show that bursting occurs in this location (Fig. 7 (b)).

4. Results and discussion

4.1. Validation of simulation results

In order to use the results of the numerical simulation, it needs to verify the results by experimental data. Four different experimental tests are carried out for verification of the simulation model. The final pressure is adjusted in a way that the bursting of the tube does not occur. Formed specimens at 25°C, 400°C and 500°C are shown in Fig. 8. The formed corner radius and thickness distribution of the 1/4 middle cross-section of the specimens are compared with the simulation results in the same loading condition (Table 3). A squared section of the specimens is cut in the peripheral direction, from the middle of the specimens to measure the wall thicknesses.

Table 2. Physical and mechanical properties of the tube.

Parameter [unit]	Amount
Young's modulus [GPa]	70
Poisson's ratio	0.3
Density [kg/m3]	2700
Thermal conductivity [W/m°C]	230
Specific heat [J/kg°C]	904
Expansion coefficient [m/m°C]	23×10^{-6}

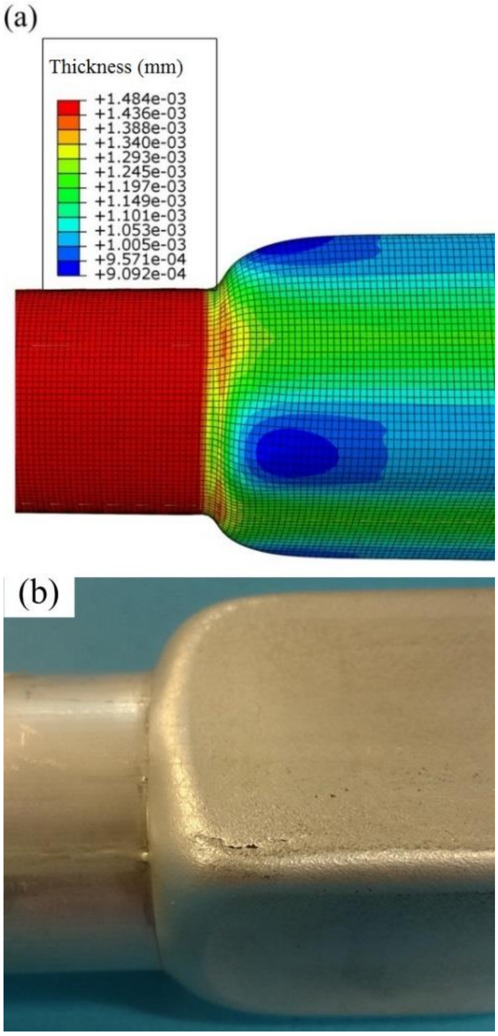

Fig. 7. Formed part at 500°C and maximum internal pressure of 12 bar; (a) simulation; (b) experiments

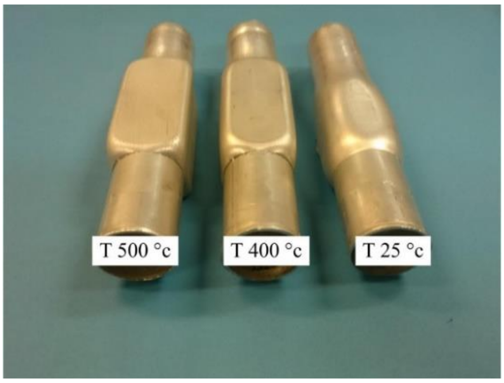

Fig. 8. Specimens produced in temperatures of 25°C, 400°C and 500°C.

Then, wall thickness is measured by a micrometer, as shown in Fig. 9(a). The changes in the wall thickness of the tubes, in experiments and numerical simulations, after processing at the temperatures of 25°C, 400°C, and 500°C are shown in Fig. 9(b). The maximum differences of the thickness distribution, between simulation and experimental results, in the temperatures of 25°C, 400°C, and 500°C are 2.4%, 4.55%, and 5.04%, respectively. In fact, with the increasing temperature, the error percentage for prediction of the corner radius and thickness distribution increases. Because, as the temperature increases, heat transfer of the setup to the environment increases, and so its control becomes more difficult in the experiments. Thus, the temperature distribution in the sections of the specimen becomes more non-uniform.

Further experimentation is carried out by changing the time period of the process. Two specimens is formed at the temperature of 500°C and pressure of 10 bar, according to two time periods of 30 s and 90 s (Fig. 10).

Table 3. Numerical and experimental result comparison.

Process temperature [°C]	Gas pressure [bar]	Radius (simulation) [mm]	Radius (experiment) [mm]	Error [%]
25	157	19.98	19.4	3
400	20	6.81	6.5	4.76
500	12	6.01	5.7	5.44

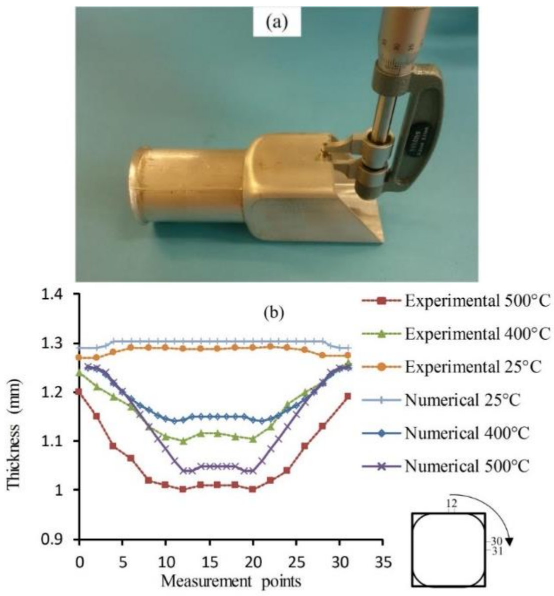

Fig. 9. (a) Measuring wall thickness in the middle cross-section; (b) thickness distribution of specimens in simulations and experiments.

Table 4. Numerical and experimental result comparison for different time periods.

Process temperature [°C]	Gas pressure [bar]	Process time [s]	Radius (simulation) [mm]	Radius (experiment) [mm]	Error [%]
500	10	30	7.97	7.6	4.86
500	10	90	7.3	7	4.28

Numerical simulations are conducted with the same conditions as experiments and the obtained radii are compared. Table 4 compares the experimental and numerical results. Results show that the finite element method could be used for the prediction of the deformation in the HMGF of AA6063 tubes.

4.2. Effect of process temperature on pressure

The results of the uniaxial tensile test show that with increasing temperature from 25°C to 500°C, yield stress reduces significantly. Therefore, the required deformation force of the process decreases, and the final shape could be formed by lower gas pressure. The minimum required pressure for obtaining the minimum corner radius in the tubes (without bursting) at three different temperatures of 25°C, 400°C and 500°C are illustrated in Fig. 11. It shows the increasing process temperature from 25°C to 400°C, and 500°C, decreases the required internal pressure of the gas in the factor of 87.2 % and 92.3% respectively.

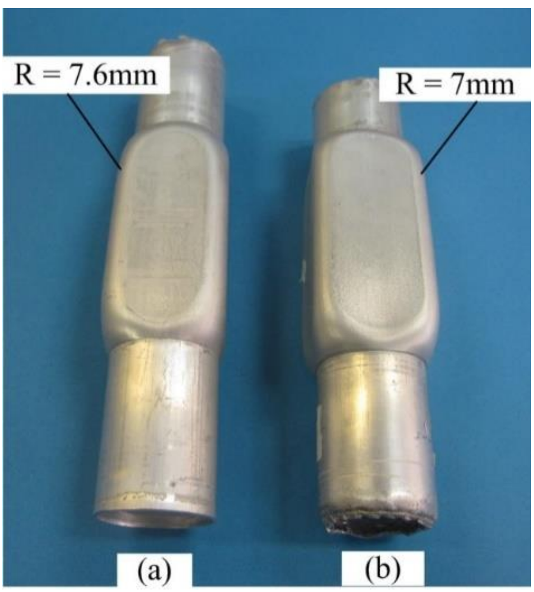

Fig. 10. Specimens produced at different time periods of process; (a) 30 s and (b) 90 s.

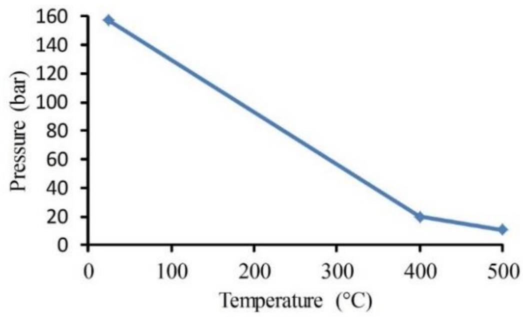

Fig. 11. Required forming pressure in different temperatures.

In fact, the internal pressure required to achieve the corner radius of 19.4 mm at 25°C is equal to 157 bar, while at temperatures of 400°C and 500°C (for producing corner radius of 6.5 mm and 5.7 mm, respectively) the required pressure reduces to 20 bar and 12 bar, respectively. This leads to the possibility of using a lower capacity press machine to seal the tube ends, reducing the clamping force of the die, as a consequence, reducing the cost of dies and components. In addition, internal pressure can be provided by simpler procedures; hydraulic pumps are utilized to supply the high forming pressures in the Hydroforming process, while the gas cylinder is sufficient in the HMGF process. Also, lower applied forming pressure makes this process safer process compared to other processes.

4.3. Effect of process temperature on the formed radius

The corner radius of the square parts is one of the significant outputs of the process. As the radius corner decreases, it means the specimen has a more detailed square-shaped. The results indicates that with increasing the process temperature, the fracture strain increases, flow stress decreases, and the effect of work-hardening decreases as well, thus a smaller corner radius achieves. Fig. 12 shows the corner radius at the ambient temperature is equal to 19.98 mm, while HMGF at the temperatures of

400°C and 500°C, reduces the corner radius of the products 66.48% and 69.91%, respectively. The results show that the mechanical behavior of AA6063 alloy is similar to superplastic materials as the temperature increases. Thus, complex shapes and small-radius corners could be produced at elevated temperatures.

4.4. Effect of temperature on the thickness distribution

The thickness of the final products is considered a geometrical criterion, which indicates the quality of the products. Fig. 13 illustrates the thickness changes of the tube cross-section, in the middle of the specimen, at three temperatures of 25°C, 400°C, and 500°C. As it shows, the thinning is low and the thickness distribution is more uniform at ambient temperatures, due to the low plastic deformation in the specimen. The minimum thickness of the tube wall is 1.29 mm.

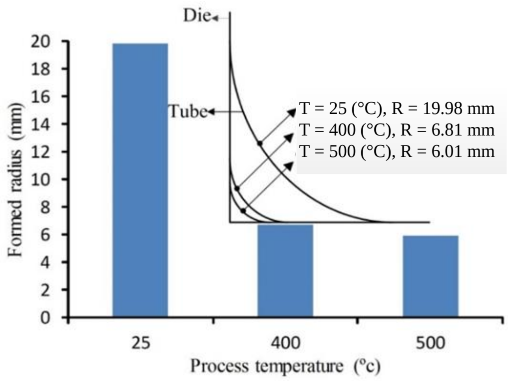

Fig. 12. Effect of process temperature on the formed corner radius.

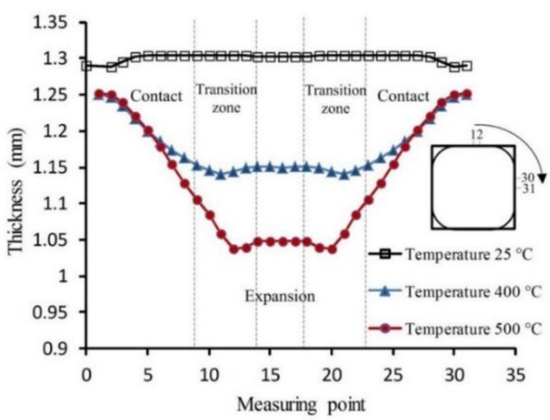

Fig. 13. Thickness distribution in different temperatures.

On the other hand, when the temperature reaches 400°C and 500°C, the values of deformation enhances and the square corners experiences a more deformation. In fact, the material flows from the points (which are in contact with the die) to the corners. Because of the lack of axial feeding, the thickness reduces significantly and the minimum thickness reaches to 1.14 mm, and 1.04 mm at 400°C and 500°C, respectively. Also, the minimum thickness occurs in the transition zone (Fig. 13). The transition zone is a part of the tube wall, in which the tube loses its contact with the die surface.

Fig. 14 illustrates the changes in the thickness in the middle cross-section of the tube, during the process at 500°C and a pressure of 12 bar. First, the thickness of the specimen decreases uniformly and the tube bulges freely. In this step, the specimen has not any contact with the die, and there is no friction between specimen and die. By increasing internal pressure, the specimen deforms more and therefore, contacts with the die surfaces. Thickness starts to change non-uniformly (i.e. from the pressure of 5.8 bar); when the specimen touches the die due to the friction between tube wall and die surface. Thus, the material flows hardly where the specimen has contact with the die, and the thickness does not change very much because of the existing friction between the die and external surface of the tube. Consequently, the final thickness of the specimen in these areas is much greater than the other. On the other hand, the area without any contact with the die expands freely and becomes thin. This area needs to be fed from the part of the tube which has a contact with the die. However, the material in the contact zone has a difficult flow to the free expanding parts, due to the friction.

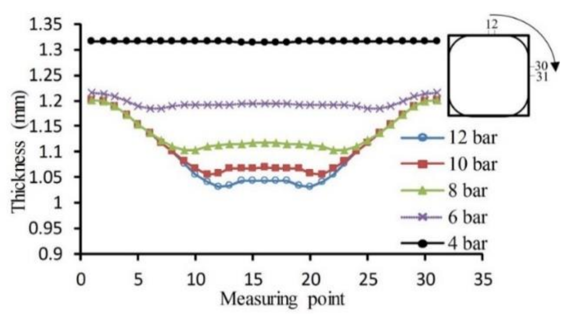

Fig. 14. Changing of the thickness distribution during the process.

As a result, the free expanding zone becomes thinner, compared to the parts which have contact with the die. The transition zone (i.e. the boundary between the expanding area and the area that has contact with the die) is under the effect of two opposite direction forces; (1) the forming force applied to this area because of the expansion; and (2) the friction force applied in an opposite direction, which inhibits the material from flowing. The interaction between these two forces induces more tensile stress rather than other parts in the peripheral direction of the transition zone.

Fig. 15 shows stress and thickness distribution in the peripheral direction when a temperature of 500°C and a pressure of 12 bar is applied to the tube. Since the values of stress in the transition zone is greater than the other areas, the zone reaches the ultimate stress sooner and becomes thinner than the other areas.

4.5. Effect of time period of the process

When the time period of the forming increases, the rate of internal pressurizing of the gas decreases. The strain rate effects on the flow stress of the material at elevated temperatures. In the condition of decreasing strain rate and high temperatures applied to AA6063 tubes, the value of fracture strain increases and the material is able to be formed more. Numerical simulations at a temperature of 500°C and a pressure of 10 bar and different time periods are carried out. The results shown in Fig. 16 depict that with an increase in the time period of the process from 30 s to 90 s, the formability of the material.

4.6. Effects of the loading path

4.6.1. Constant pressure in the end of process

When the process is performed with constant pressure at room temperatures, the amount of the corner radius does not change. Because of the hard-working phenomenon, the yield stress increases, and thus higher pressures are required to form the tube more. Recall that for AA6063 at elevated temperatures of 400°C and 500°C, the effect of hard-working assumes to be negligible, and the strain increases when the stress is applied in a constant magnitude (Fig. 2).

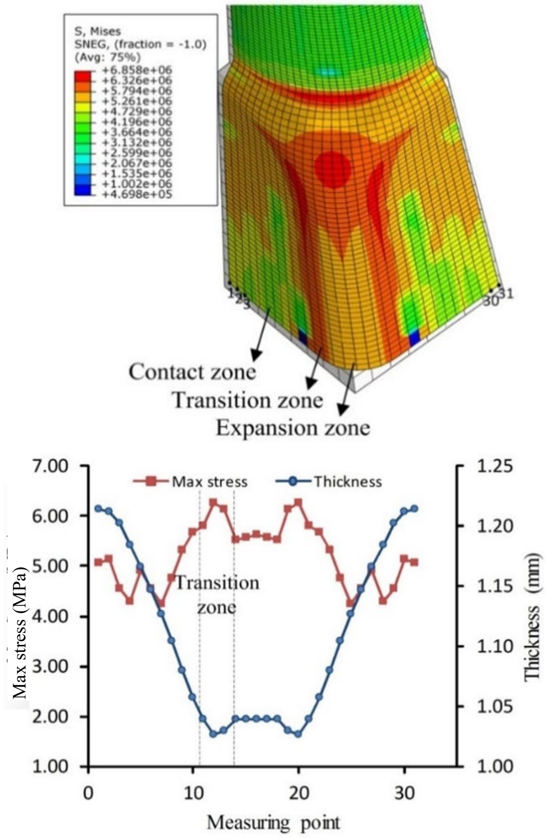

Fig. 15. Stress and thickness distribution in the middle of final specimen.

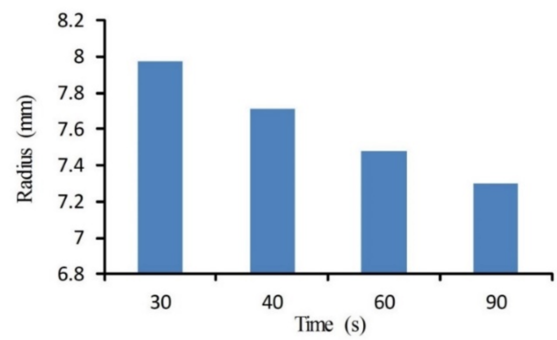

Fig. 16. Effect of time period of forming process on formed radius.

In addition, stress is a function of strain rate at high temperatures, and strain rate reduces after a little plastic deformation occurs (i.e. stress reaches its maximum and becomes constant). As shown in Fig. 2, decreasing the strain rate reduces the yield stress of the material.

The changes in the corner radius during the process are illustrated in Fig. 17. In the first step of the process, the pressure reaches its maximum value within 20 s, and in the second step, it becomes steady up to the end of the process. In the first step, the radius increases slowly during the initial elastic deformation. However, the changes in the corner radius increase rapidly during the consequence of plastic deformation. The radius increases with a constant rate and the specimen expands uniformly until it touches the die. Then, the radius amount starts to reduce (i.e. when the pressure reaches its highest value of 12 bar, the corner radius is 7.17 mm). In the second stage, the changes of the corner radius become lower when the time passes, and reaches 5.99 mm within 80 s in the constant pressure of 12 bar (that is, corner radius reduces 16.5% during the second step).

4.6.2. Different loading paths

The loading path is one of the effective parameters in the HMGF process. For investigating the effect of this parameter on the formability of the material, different loading paths are applied at a temperature of 500°C and a pressure of 12 bar (Fig. 18). Also, the changes in the corner radius during the forming process regard to different loading paths are shown in Fig. 19. As it shows, the maximum deformation and minimum corner radius belong to the loading path #2 (the corner radius formed is 5.47 mm). In addition, the maximum value of the corner radius is 6.3 mm and belongs to the loading path #4.

Fig. 20 shows the history of strain and strain rate during the process for different loading paths (in a point which has the lowest amount of thickness). For the loading path #2, the pressure is applied with the largest rate, and therefore, the strain rate is high (Fig. 20). Thus, the tube bulges freely, and the thinning of the tube occurs uniformly along the perimeter of the tube. Considering the fixed process time (i.e. 30 s), the shorter the time of free bulging, the more the time to form the tube corners at the second part of the loading path. As shown in Fig. 20, when the corners are formed, the lowest amount of strain rate appears in loading path #2, due to having more time in this step. Moreover, the fracture strain increases with decreasing the strain rate. As a consequence, the tube forms more and the corner radius becomes smaller. Loading path #1, in which the pressure increases with a constant slope, has a higher strain rate, and because the fracture strain decreases, the consequent corner radius is less than that of in loading path #2.

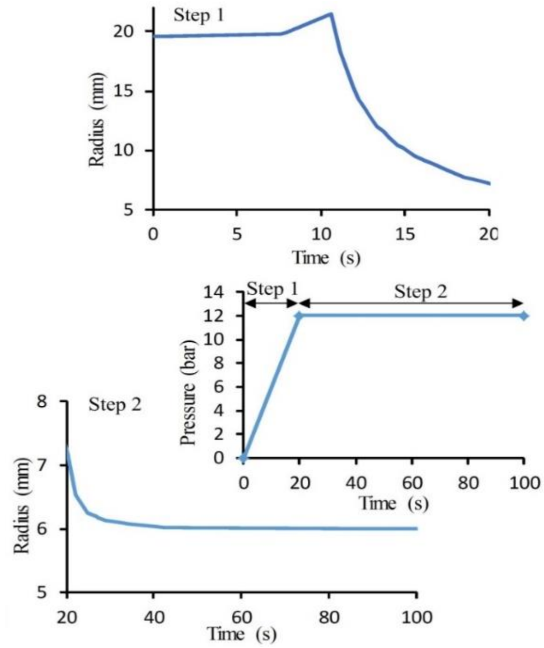

Fig. 17. Changes of corner radius during process.

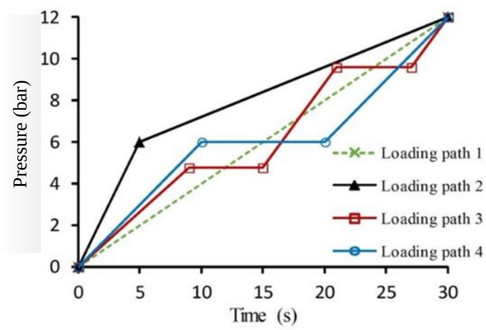

Fig. 18. Different loading paths.

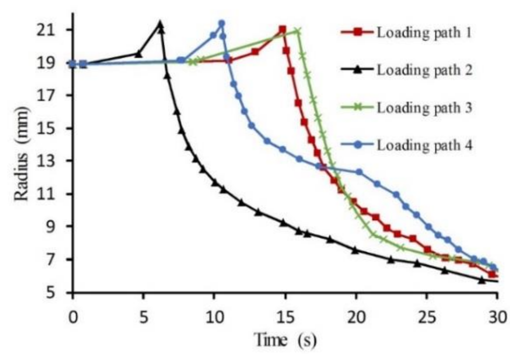

Fig. 19. Changes of corner radius during forming process for different loading paths.

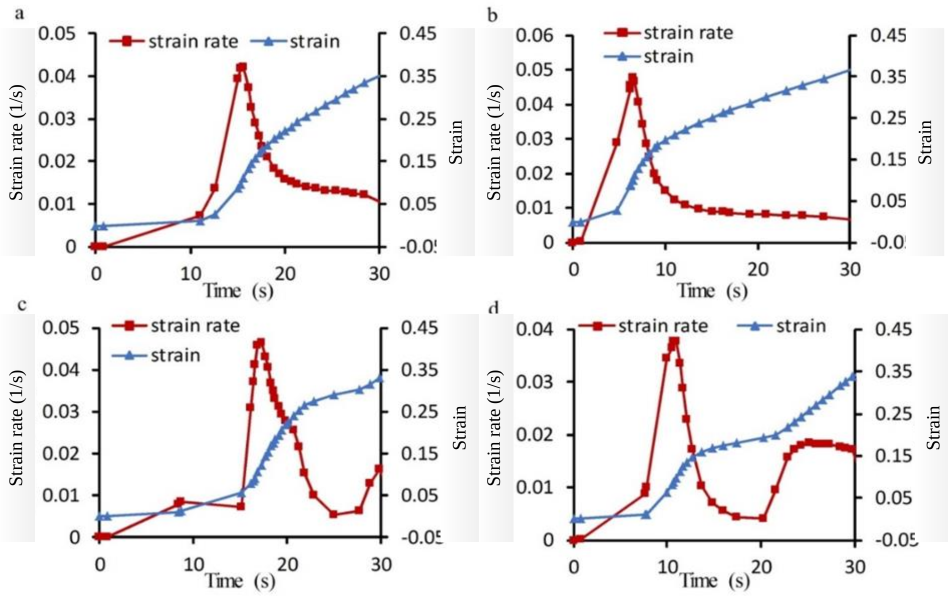

Fig. 20. History of strain and strain rate during the forming process for different loading paths; (a) path #1; (b) path #2; (c) path #3; (d) path #4.

Finally, in loading paths #3 and #4, there is a constant pressure section during the process. When the pressure is constant, strain increases with a lower slope; therefore, a low amount of the deformation occurs. Moreover, in other times when the pressure is not constant, it increases with a higher slope. Consequently, with increasing strain rate, the ultimate strain increases.

5. Conclusions

In this paper, aluminum AA6063 tubes with a square cross-section are produced, using the hot gas forming process. Different loading conditions are studied at elevated temperatures to obtain the maximum value of formability and minimum corner radius. The results show that with increasing the temperature the formability of the material increases and a lower corner radius is formed. In fact, the thinning in the transition zone is maximized, and it limits formability. By increasing the process time period, the strain rate becomes smaller and lower corner radii could be obtained. At the elevated temperatures, the forming process of the tube continues in constant pressure, because of the superplastic behavior of the material. Also, the lower amount of corner radius is achieved. By increasing the time of loading, it is possible to decrease the corner radius by the factor of 8.4 % at 500°C. Furthermore, it is observed that the maximum amount of forming could be obtained, if the internal pressurizing rate of the process increases at the initial step (i.e. during the bulging of the tube). In the next step (when the corner radius is to be formed), the rate of gas pressurizing should be decreased.

References

[1] Z. B. He, B. G. Teng, C. Y. Che, Z. B. Wang, K. L. Zhengl and S. J. Yuan, “Mechanical properties and formability of TA2 extruded tube for hot metal gas forming at elevated temperature”, *Transactions of Nonferrous Metals Society of China*, Vol. 22, No. 1, pp. 479-484, (2012).

[2] J. Jeswiet, M. Geiger, U. Engel, M. Kleiner, M. Schikorra, Joost Duflou, R. Neugebauer, P. Bariani and S. Bruschi, “Metal forming progress since 2000”, *CIRP Journal of Manufacturing Science and Technology*, Vol.1, No. 1, pp. 2-17, (2008).

[3] S. Novotny and M. Gieger, “Process design for hydroforming of lightweight metal sheets at elevated temperatures”, *Journal of Materials Processing Technology*, Vol. 138, No. 1-3, pp.594-599, (2003).

[4] Z. B. H3, X. B. Fqan, S. Fei, K. L. Zheng, Z. B. Wang and S. J. Yuan, "Formability and microstructure of AA6061 Al alloy tube for hot metal gas forming at elevated temperature", *Transactions of Nonferrous Metals Society of China*, Vol. 22, No. 1, pp. 364-369, (2012).

[5] M. Keigler, H. Bauer, D. Harrison and A. K. De Silva, "Enhancing the formability of aluminium components via temperature controlled hydroforming", *Journal of Materials Processing Technology*, Vol. 167, No. 2-3, pp. 363-370, (2005).

[6] H. Yi, E. Pavlina, C. Van Tyne and Y. Moon, "Application of a combined heating system for the warm hydroforming of lightweight alloy tubes", *Journal of materials processing technology*, Vol. 203, No. 1-3, (2008).

[7] Z. He, S. Yuan, G. Liu, J. Wu and W.Cha, "Formability testing of AZ31B magnesium alloy tube at elevated temperature", *Journal of Materials Processing Technology*, Vol. 210, No. 6-7, pp.877-884, (2010).

[8] S. J. Hashemi, H. M. Naeini, Gh. Liaghat, R. Azizi Tafti and F. Rahmani, "Numerical and experimental investigation of temperature effect on thickness distribution in warm hydroforming of aluminum tubes", *Journal of Materials Engineering and Performance*, Vol. 22, No. 1, pp.57-63, (2013).

[9] B. J. Kim, C. J. Van Tyne, M. Y. Lee and Y. H. Moon, "Finite element analysis and experimental confirmation of warm hydroforming process for aluminum alloy", *Journal of Materials Processing Technology*, Vol. 187, No. 1, pp.296-299, (2007).

[10] S. J. hashemi, *Prediction of Forming Limit Diagram in Warm Tube Hydroforming Using Ductile Fracture Criteria*, PhD. Thesis.

[11] N. Abedrabbo, F. Pourboghrat and J. Carsley, "Forming of AA5182-O and AA5754-O at elevated temperatures using coupled thermo-mechanical finite element models", *International Journal of Plasticity*, Vol. 23, No. 5, pp. 841-875, (2007).

[12] H. Choi, M. Koc and J. Ni, "A study on warm hydroforming of Al and Mg sheet materials: mechanism and proper temperature conditions", *Journal of Manufacturing Science and Engineering*, Vol. 130, No. 4, pp. 041007, (2008).

[13] T. Naka, G. Torikai, R. Hino and F. Yoshida, "The effects of temperature and forming speed on the forming limit diagram for type 5083 aluminum–magnesium alloy sheet", *Journal of Materials Processing Technology*, Vol. 113, No.1-3, pp.648-653, (2001).

[14] R. Verma, L. G. Hector, P. E. Krajewski and E. M. Taleff, "The finite element simulation of high-temperature magnesium AZ31 sheet forming", *Jom*, Vol. 61, No. 8, pp. 29-37, (2009).

[15] T. Maeno, K. I. Mori and K. Fujimoto, "Hot gas bulging of sealed aluminium alloy tube using resistance heating", *Manufacturing Review*, Vol. 1, No. 1, pp.1, (2014).

[16] T. Maeno, K. I. Mori and C. Unou, "Improvement of die filling by prevention of temperature drop in gas forming of aluminium alloy tube using air filled into sealed tube and resistance heating", *Procedia Engineering*, Vol. 81, No. 1, pp. 2237-2242, (2014).

[17] Y. Lee, J. J. Kim, Y. N. Kwon and E. Y. Yoon, "Formability and Grain Size of AZ31 Sheet in Gas Blow Forming Process", *Procedia Engineering*, Vol. 81, No.1, pp. 748-753, (2014).

[18] A. Paul and M. Strano, "The influence of process variables on the gas forming and press hardening of steel tubes", *Journal of Materials Processing Technology*, Vol. 228, No. 1, pp. 160-169, (2015).

[19] Y. Wu, G. Liu, K. Wang, Z. Liu and S. Yuan, "The deformation and microstructure of Ti-3Al-2.5 V tubular component for non-uniform temperature hot gas forming", The International *Journal of Advanced Manufacturing Technology*, Vol. 88, No. 5-8, pp. 1-10, (2016).

[20] Y. Wu, G. Liu, K. Wang, Z. Liu and S. Yuan, "Loading path and microstructure study of Ti-3Al-2.5 V tubular components within hot gas forming at 800°C", The International *Journal of Advanced*

Manufacturing Technology, Vol. 87, No. 5-8, pp. 1-11, (2016).

[21] W. J. Kim, W. Y. Kim and H. K. Kim, "Hot-air forming of Al-Mg-Cr alloy and prediction of failure based on Zener-Holloman parameter", *Metals and Materials International*, Vol. 16, No. 6, pp.895-903, (2010).

[22] X. Fan, Z. He, P. Lin and S. Yuan, "Microstructure, texture and hardness of Al–Cu–Li alloy sheet during hot gas forming with integrated heat treatment", *Materials & Design*, Vol. 94, No. 1, pp.449-456, (2016).

[23] K. Wang, G. Liu, J. Zhao, J. Wang and S.Yuan, "Formability and microstructure evolution for hot gas forming of laser-welded TA15 titanium alloy tubes", *Materials & Design*, Vol. 91, No. 1, pp.269-277, (2016).

[24] G. Wang, K. F. Zhang, D. Z. Wu, J. Z. Wang and Y. D. Yu, "Superplastic forming of bellows expansion joints made of titanium alloys", *Journal of Materials Processing Technology*, Vol. 178, No. 1-3, pp.24-28, (2006).

[25] R. Neugebauer and F. Schieck, "Active media-based form hardening of tubes and profiles", *Production Engineering*, Vol. 4, No. 4, pp.385-390, (2010).

[26] G. Liu, J. Wang, K. Dang and Z. Tang, "High pressure pneumatic forming of Ti-3Al-2.5 V titanium tubes in a square cross-sectional die", *Materials*, Vol. 7, No. 8, pp.5992-6009, (2014).

[27] G. Liu, Y. Wu, D. Wang and S. Yuan, "Effect of feeding length on deforming behavior of Ti-3Al-2.5 V tubular components prepared by tube gas forming at elevated temperature", *The International Journal of Advanced Manufacturing Technology*, Vol. 81, No. 9-12, pp.1809-1816, (2015).

[28] T. Maeno, K. Mori and C. Unou, "Optimisation of condition in hot gas bulging of aluminium alloy tube using resistance heating set into dies", *Key Engineering Materials*, Vol. 473, No. 1, pp. 69-74, (2011).

[29] L. Vadillo, M. T. Santos, M. A. Gutierrez, I. Pérez, B. González and V. Uthaisangsuk, "Simulation and experimental results of the hot metal gas forming technology for high strength steel and stainless steel tubes forming", *AIP Conference Proceedings*, vol. 908, No. 1, pp. 1199-1204, (2007).

[30] M. Rajaee, S. J. Hosseinipour and H. Jamshidi Aval, "Tearing criterion and process window of hot metal gas forming for AA6063 cylindrical stepped tubes", *The International Journal of Advanced Manufacturing Technology*, (2018).

[31] Y. Wu, G. Liu, Z. Liu and B. Wang, "Formability and microstructure of Ti22Al24. 5Nb0. 5Mo rolled sheet within hot gas bulging tests at constant equivalent strain rate", *Materials & Design*, Vol. 108, No. 1, pp.298-307, (2016).

[32] A. T. Anaraki, M. Loh-Mousavi and L. L. Wang, , "Experimental and numerical investigation of the influence of pulsating pressure on hot tube gas forming using oscillating heating", *The International Journal of Advanced Manufacturing Technology*, Vol. 97, No. 9-12, pp.1-10, (2018).

How to cite this paper:

M. Nasrollahzade, S. J. Hashemi, H. Moslemi Naeini, Amir H. Roohi and Sh. Imani Shahabad, "Investigation of hot metal gas forming process of square parts", *Journal of Computational and Applied Research in Mechanical Engineering*, Vol. 10, No. 1, pp. 125-138, (2020).

DOI: 10.22061/jcarme.2019.3914.1457

URL: http://jcarme.sru.ac.ir/?_action=showPDF&article=1044